Growth front roughening in silicon nitride films by plasma-enhanced chemical vapor deposition

T. Karabacak,* Y.-P. Zhao, G.-C. Wang, and T.-M. Lu
Department of Physics, Applied Physics and Astronomy, Rensselaer Polytechnic Institute, Troy, New York 12180-3590
(Received 18 October 2001; revised manuscript received 18 April 2002; published 22 August 2002)

The dynamic roughening of amorphous silicon nitride growth front prepared by a plasma-enhanced chemical vapor deposition is presented. Morphology of the films grown at different substrate temperatures (from 50 to 350 °C) for various lengths of deposition time was measured *ex situ* using atomic force microscopy. The dynamic scaling exponents are measured as $\alpha \sim 0.77$, $\beta \sim 0.40$, and $1/z \sim 0.28$, and do not change significantly under the investigated substrate temperature range. An attempt has been made to describe the plasma growth process using a multiparticle reemission model where the incident flux distribution, sticking coefficient, shadowing, surface diffusion, and desorption mechanisms all contributed to the growing morphology.

DOI: 10.1103/PhysRevB.66.075329 PACS number(s): 68.35.Ct, 68.55.Jk, 81.15.Aa, 68.35.Fx

I. INTRODUCTION

Silicon nitride thin films deposited by plasma-enhanced chemical vapor deposition (PECVD) have been studied for over 3 decades and are widely used in the semiconductor industry. Most of the studies focused on the solar cell applications and thin-film transistors (TFT), where silicon nitride has been used as a passivation coating, a diffusion barrier, a gate dielectric, and an interlevel metal isolation. The composition and properties of PECVD silicon nitride films vary widely with deposition conditions and hundreds of studies have been reported. Most studies concern the composition or the physical properties, such as electrical properties, of these films as a function of deposition conditions. Only a few studies reported the reactions occurring in the plasma and on the deposition surface.[1–7]

In thermal CVD, gas-phase reactive species are generated by heating the initial reactants. In plasma CVD, the plasma energy supplied by an external rf source takes the place of heating to generate the species that subsequently react and deposit on substrate surfaces. Excessive heating and degradation of a substrate can be significantly avoided by using plasma electron kinetic energy instead of thermal energy. When the plasma is initiated, energy from the rf electric field is coupled into the reactant gases via the kinetic energy of a few free electrons. These electrons gain energy rapidly through the electric field and lose this energy slowly through inelastic collisions. The high-energy electrons are capable of making inelastic collisions that cause the reactant gas molecules to dissociate and ionize, producing secondary electrons by various electron-impact reactions. The two important aspects of a plasma glow discharge are the nonequilibrium low-temperature gas-phase chemical reactions that generate radical and ion reactive species in the plasma discharge, and the flux and energy of these reactive species as they reach and strike the surface of the film being deposited. The bombardment of the ionic species on the surface of the film, which controls the surface mobility of the precursor, is the predominant factor in determining film composition, density, stress, and step coverage or conformality at relatively low temperatures used in plasma CVD.[6]

Reactions during plasma deposition are complex and are not understood completely. Elementary reactions that occur in a plasma have been discussed by various authors.[8–11] In general, the deposition mechanisms for a plasma CVD process can be qualitatively divided into four major steps. Step 1 includes the primary initial electron-impact reactions between electron and reactant gases to form ions and radical reactive species. In step 2, transport of these reactive species occurs from the plasma to the substrate surface concurrently with the occurrence of many elastic and inelastic collisions in both the plasma and sheath regions, classified as ion and radical generation steps.[12] Step 3 is the absorption and/or reaction of reactive species (radical absorption and ion incorporation) onto the substrate surface. Finally, in step 4, the reactive species and/or reaction products incorporate into the deposited films or reemit from the surface back to the gas phase. Due to their complexity, the latter two steps are the least known and least studied aspects of plasma CVD. Significant roles are played by ion bombardment[13,14] and various heterogeneous reactions between ions and radicals with the depositing surface in the sheath region. The first two steps critically affect film properties such as conformality,[15,16] density, stress,[13] and "impurity" incorporation. However, the later two steps will greatly affect the surface morphology and the chemical compositions of the film.

Thus far there has been no report on how these complex reactions affect the morphology of plasma-deposited thin films. A previous single-particle reemission growth model was proposed by Drotar *et al.* but the surface diffusion and desorption were not included.[17,18] In a recent study we proposed a similar growth model for amorphous silicon by magnetron sputtering.[19] The model was also single particle and did not include desorption, which was not significant for the sputtering growth conditions. In the present work, we report measurements of growth front roughness of silicon nitride films grown by a PECVD method. We propose a more complex, multiparticle reemission growth model that includes sticking coefficient, shadowing, surface diffusion, and desorption mechanisms to describe the morphology evolution of PECVD growth of silicon nitride films. Using scaling theories[20–22] we attempt to describe possible surface growth mechanisms during a PECVD deposition.

 ©2002 The American Physical Society

TABLE I. Growth rate, composition, and roughness parameters obtained from experiments and simulations at different substrate temperatures. rf power is set to 32 W.

Temperature (°C)		50	150	250	350
Growth rate (nm/min)		6.08±0.08	5.72±0.09	4.70±0.07	4.39±0.11
Hydrogen concentration (%)		28±1	27±1	23±1	18±1
β	Experimental	0.41±0.02	0.41±0.01	0.38±0.02	0.42±0.02
	Simulation	0.40±0.01	0.37±0.01	0.39±0.01	0.43±0.02
α	Experimental	0.81±0.02	0.78±0.02	0.76±0.04	0.80±0.03
	Simulation	0.48±0.02	0.46±0.02	0.47±0.02	0.51±0.02
$1/z$	Experimental	0.29±0.03	0.28±0.02	0.28±0.03	0.16±0.02
	Simulation	0.57±0.02	0.59±0.02	0.60±0.01	0.61±0.02
Si/N ratio	Experimental	1.250±0.050	1.250±0.050	1.125±0.045	1.200±0.048
	Simulation	1.227±0.010	1.208±0.010	1.200±0.010	1.192±0.010

II. EXPERIMENTAL RESULTS

The silicon nitride films were deposited in a Plasma Therm© Model 70 using a flow of SiH_4/N_2/He mixtures to generate the plasma. Process conditions during the deposition were as follows. The total deposition pressure was 0.89 Torr, the rf power was 32 W (which corresponds to 0.032 W/cm for our system), and the rf was 13.56 MHz. Flow rates for SiH_4, N_2, and He were 10, 478, and 1572 cubic centimeter per min at STP, respectively. We used the front side of Si(100) wafers, which were RCA cleaned prior to deposition, as the substrate surface. Depositions were made at substrate temperatures of 50, 150, 250, and 350 °C. For each substrate temperature, films were grown at deposition durations ranging from 10 min up to 3 h. After each growth, film thickness was measured using a Nanoscope©. The growth rates are listed in Table I. Figure 1 plots the growth rate R as a function of the substrate temperature T_s. In Fig. 1, we show the measured growth rates for different rf powers at 50 °C and 0.89 Torr. Growth rate increases with rf power up to ~120 W, after that it does not change significantly. We will see in the following section that the rate-power relation can give some clues about the species forming in the plasma.

Since the SiN film is a multicomponent film involving three different gases in the deposition, it is very important for us to know the relative concentration of different chemical components in the film in order to better understand the film deposition mechanisms. In order to obtain hydrogen concentrations, we performed nuclear reaction analysis (NRA) measurements on the as-deposited films. The average H concentrations for different substrate temperatures are summarized in Table I. The average silicon to nitrogen ratios were obtained from Rutherford backscattering (RBS) analysis, as shown in Table I. Clearly, as the substrate temperature increases, both the H concentration and the Si/N ratio decrease.

The surface morphology was measured using contact-mode atomic force microscopy (AFM). The radius of the Si_3N_4 tip is about 10 nm, and the side angle is about 10°. Representative surface morphologies are shown in Fig. 2 for the growth times of $t=25$, 75, 120, and 180 min at substrate temperature $T_s=250\,^\circ\mathrm{C}$ and growth rate $R=4.70\pm0.07$ nm/min. As can be seen from Fig. 2, the overall surface features enlarge with the increase in growth time.

The quantitative information of the surface morphology can be extracted from the equal-time height-height correlation function $H(r,t)$, defined as $H(r)=\langle[h(\mathbf{r})-h(0)]^2\rangle$. The function $h(\mathbf{r})$ is the surface height at position $\mathbf{r}[=(x,y)]$ on the surface. The notation $\langle\cdots\rangle$ means a statistical average. The scaling hypothesis requires that $H(r)\sim r^{2\alpha}$ for $r\ll\xi$, and $H(r)=2w^2$ for $r\gg\xi$.[1–7] Here ξ is the lateral correlation length, w is the interface width or rms roughness, and α is the roughness exponent, which is directly related to the surface fractality. Under the dynamic scaling hypothesis, the interface width w increases as a power law of film thickness d, $w\sim d^\beta$, where β is the growth exponent, and the lateral correlation length ξ grows as $\xi\sim d^{1/z}$, where $1/z$ is the dynamic exponent. Dynamic scaling also requires that $z=\alpha/\beta$. Therefore, from the slopes of linear fits to the log-log plots of $H(r)$ versus r (for $r\ll\xi$), w versus d, and ξ versus d,

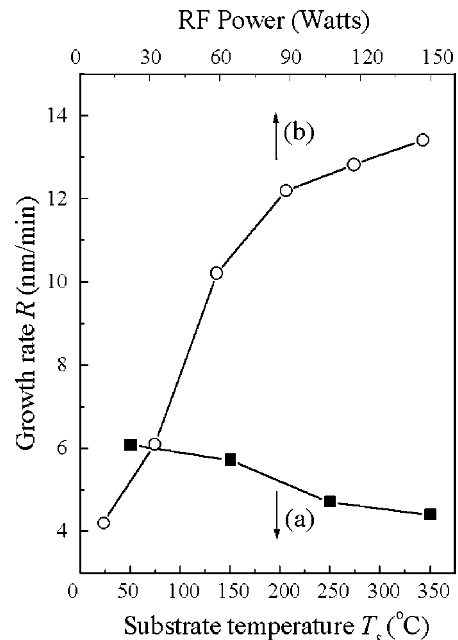

FIG. 1. (a) Growth rate R at different deposition temperatures. rf power is set to 32 W. (b) Growth rate R at different rf powers. Deposition temperature is set to 50 °C.

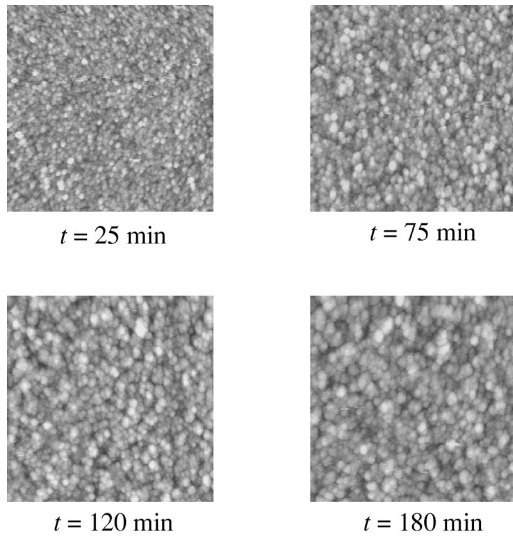

FIG. 2. Four representative surface morphologies ($2\times 2\ \mu m^2$) measured by AFM for growth times of $t=25$, 75, 120, and 180 min at the substrate temperature $T_s=250\,°C$, rf power 32 W, and growth rate $R=4.70\pm 0.07$ nm/min.

we can extract the roughness exponents α, β, and $1/z$, respectively.

In Fig. 3, we plot the height-height correlation functions of SiN films in log-log scale for $T_s=50$, 150, 250, and 350 °C. Clearly the overall behaviors of $H(r,t)$ are similar. For small lateral length the height-height correlation func-

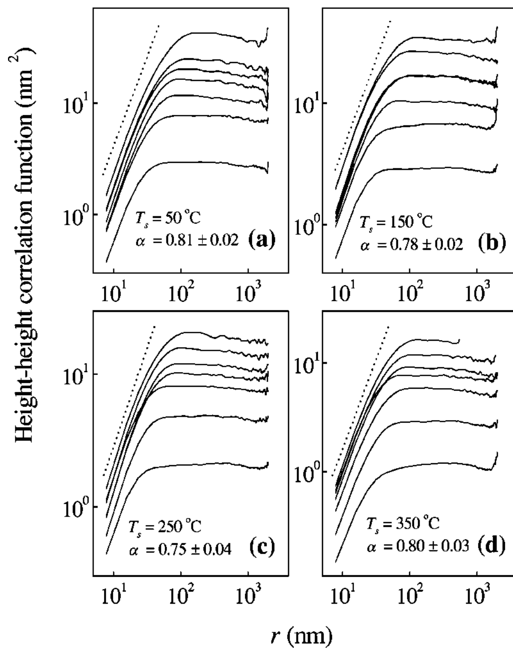

FIG. 3. The equal-time height-height correlation function $H(r,t)$ as a function of the distance r is plotted in log-log scale for $T_s=50$, 150, 250, and 350 °C in (a), (b), (c), and (d), respectively. In each graph, the $H(r,t)$ curves corresponding to 10, 25, 45, 75, 90, 120, and 180 min deposition times start from the lowest level then move up. Each $H(r,t)$ within the short-range spatial scaling regime gives the same α value indicated as the dashed line.

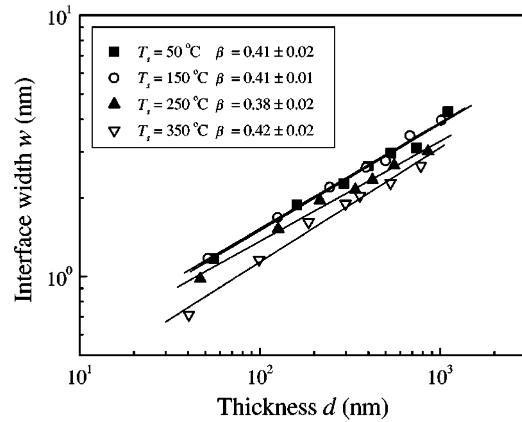

FIG. 4. The interface width w versus film thickness d at different deposition temperatures is plotted in log-log scale. At different deposition temperatures, the log-log plots are almost parallel, indicating similar β values.

tions do not overlap, which implies that the growth is not stationary, i.e., the local slope is a function of the growth time.[23] As can be seen from Table I the roughness exponents have almost equal values within experimental errors. The average roughness exponent α from all four deposition temperatures is 0.77 ± 0.03. The measured α values can be higher than the true values because of the tip effect, which will be discussed later.[24]

The interface width w and the lateral correlation length ξ versus film thickness d for various deposition temperatures are plotted in Figs. 4 and 5, respectively. For different deposition temperatures, the log-log plots of w versus d are almost parallel to each other, and for the same thickness d, the higher the substrate temperature T_s, the lower the w value. Similar to the observation in α values, the growth exponent β is also almost a constant value for different T_s. The β values obtained from Fig. 4 are listed in Table I. The average growth exponent from different T_s is calculated to be 0.40 ± 0.02.

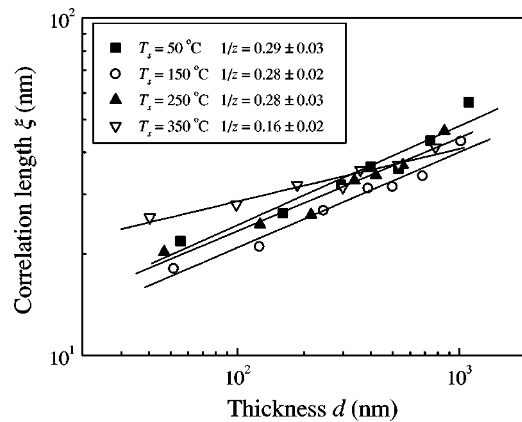

FIG. 5. The lateral correlation length ξ versus film thickness d for different deposition temperatures is plotted in log-log scale. For deposition temperatures of $T_s=50$, 150, and 250 °C the slopes are almost parallel and give similar $1/z$ values. For $T_s=350\,°C$ the slope gives a much lower $1/z$ value.

In order to determine ξ accurately, we calculated the two-dimensional autocorrelation $C(r)=\langle h(\mathbf{r})h(\mathbf{0})\rangle$ function for each AFM image, and used the quadrant circularly averaged autocorrelation function $C_c(r)$ to determine ξ by using the relation $C_c(\boldsymbol{\xi})=C_c(0)/e$. The log-log plots of ξ versus d for different deposition temperatures are also almost parallel to each other except for $T_s=350\,°\mathrm{C}$, suggesting a similar dynamic exponent $1/z$. The $1/z$ obtained from the fits to the plots in Fig. 5 are listed in Table I. The average dynamic exponent obtained (excluding $T_s=350\,°\mathrm{C}$) is 0.28 ± 0.03. For $T_s=350\,°\mathrm{C}$ we have a $1/z$ value of 0.16 ± 0.02. Using $\alpha\sim0.65$ that takes into account the tip effect and the average $\beta\sim0.40$, we obtain a dynamic exponent from the scaling relation $z=\alpha/\beta$ to be $1/z\simeq0.62$, which is not consistent with the measured value of $1/z$. This may indicate that the system does not scale based on the conventional scaling law that requires a stationary growth mechanism.

III. GROWTH MODEL

In this section we analyze our experimental data to identify possible growth mechanisms in our deposition system, and compare it with the literature.

A. Growth regime

There are two possible growth regimes in a typical (PE)CVD system: (a) diffusion-limited growth and (b) surface kinetics-limited growth.[25] Using the approximate ion, electron and neutral particle densities from the literature,[26–29] we estimated the approximate mean free path of the particles for our plasma conditions to be $\lambda\sim10^{-2}$ cm, consistent with the reported values under similar plasma conditions.[6,30,31] Assuming a feature size on the surface of the growing film $l\sim10^{-5}$ cm, we estimate the Knudsen number to be $\varkappa=\lambda/l\simeq10^{-2}/10^{-5}\simeq10^{3}\gg1$. Therefore, our deposition condition is believed to belong to the surface kinetics-limited growth regime.

B. Plasma and deposition chemistry

The role of N_2+He *dilution*. The use of N_2 as a reactant gas instead of NH_3 helps to increase the plasma density and reduces the amount of hydrogen in PECVD silicon nitride.[32,33] The hydrogen content of nitride films deposited at 250–350 °C is three times lower than that deposited with ammonia under similar conditions. Increased ion bombardment, obtained by using diluted inert gas, can also help to reduce hydrogen incorporation and to control film stress.[32,34–36]

There are speculations in the literature about the role of He in plasma chemistry.[28] Some authors suggested that He dilution may (a) prevent deexitation of active nitrogen species, and (b) act as a catalyst in Penning-type processes that influences possible reaction paths.[37–39] The resulting low reactant concentration in the plasma after He dilution tends to minimize the role of gas-phase reactions and leads to film growth conditions dominated by surface reactions. Helium may reduce the frequency of gas-phase collisions between SiH_n species and hence reduces the formation of polymeric silane species in the gas phase.[37] Helium is also believed to shield the reactive gases from fragmentation. These are believed to reduce the incorporation of impurities and produce a high-quality film structure.[5,40] The low mass of He also helps to minimize momentum transfer to the surface.[40] The film-substrate interfaces have been shown to exhibit no sign of plasma-induced damage.[41–43]

Reactive species. The concentration of reactive neutral species obtained by density calculations and optical emission and absorption techniques is about 10^4-10^5 larger than that of the ionic species.[28,44] Therefore the film deposition is dominated by neutral species, although ion bombardment can certainly modify the film structure.[44,45]

SiH_4+N_2 plasmas has been observed by means of mass spectroscopy to form no Si-N precursors,[2,3] Klein *et al.* studied PECVD hydrogenated silicon nitride films deposited from SiH_4, N_2, and He gas mixtures, and their mass spectroscopy measurements do not show any Si-N or N-H gas-phase species.[32] They suggested that N incorporation precursors are N atoms or excited N_2 molecules. Active N atoms must be produced by electron-impact dissociation in the plasma: $N_2\rightarrow N$. Mass spectroscopy shows that the amount of the N radical produced increases with plasma power and He dilution.[28,46]

Almost all the SiH_4 in a typical discharge dissociates into SiH_n $(n<4)$ even at extremely low power densities.[28] If the power is enough to dissociate all the SiH_4 to SiH_n but not enough to dissociate all N_2 to N, then some SiH_n may react with itself to form Si_2H_n by-products. This results in low deposition rates and Si-rich films.[28] The inactivated N_2 molecules do not react with the SiH_n, and instead act as inert diluents. As the power is raised, $N_2\rightarrow N$ dissociation increases, therefore both the deposition rate and N/Si ratio in the bulk of the film are expected to increase. As can be seen from Fig. 1, we have a similar change of deposition rate with rf power as stated above. Therefore at rf power of 32 W, at which we performed our experiments, we should expect the formation of Si_2H_n by-products in the plasma.

The most likely SiH_n products after electron-impact dissociation of SiH_4 are SiH_2 and SiH_3. Since we assume that approximately all SiH_4 is dissociated into SiH_n in our experiments, we do not expect $SiH_2+SiH_4\rightarrow Si_2H_6$ or $SiH_2+Si_nH_{2n+2}\rightarrow Si_{n+1}H_{2n+4}$ type of reactions to take place. Also, powder formation is not believed to be significant under our plasma conditions.[37,47,48] But, SiH_3 may react with itself to form Si_2H_6 [or through $SiH_3+SiH_3\rightarrow SiH_2+SiH_4\rightarrow Si_2H_6$ (Refs. 49 and 50)].

SiH_2 is expected to have a lower mean free path compared with SiH_3 and Si_2H_6.[47] The relative concentration of SiH_2 is also expected to be pretty low [$\sim$100 times less than that of SiH_3 (Refs. 44, 45 and 49)]. In addition, He dilution is believed to enhance the SiH_3 formation.[46] SiH_3 concentration is expected to be five to ten times larger than that of Si_2H_6.[45,49] Therefore, we suggest that the dominant species that impinge on the deposition surface in our experiments are SiH_3, Si_2H_6, and N. This is consistent with the generally accepted notion (emerging from reaction kinetics calcula-

tions, mass and optical spectroscopy measurements) that in a typical silane discharge SiH_3 is the dominant depositing species.[44,45,49,51–54]

C. Deposition and sticking coefficients

When the reactive species reach the surface, it will stick to the surface with a sticking probability. The average probability of sticking, which is called the sticking coefficient (s_c), is a result of the complicated interactions between the incident atom and the surface. s_c can range between 0 and 1. We now discuss the s_c value of the species that are believed to be dominant in our experiments.

At the initial growth time, all the SiH_3, Si_2H_6, and N species incident on hydrogen-free Si substrate surface are expected to have sticking coefficients approximately equal to unity.[2,3,55] Hydrogen forms a strong bond with the surface atom and passivate it against any adsorption, and therefore results in lower sticking coefficients for other species that arrive subsequently.[47]

SiH_3 specie is a monoradical with only one dangling bond, and therefore cannot be added to fully hydrogenated sites. Instead, it can only react with an unterminated silicon or nitrogen dangling bond (e.g., $\equiv$Si— $+SiH_3 \rightarrow \equiv$Si $-SiH_3$).[56] Perrin and Broekhuizen measured the sticking coefficient of SiH_3 on an a-Si:H surface at various substrate temperatures (they used a grid system to calculate the sticking coefficients).[49,50] We adopt their results and set the sticking coefficient of SiH_3 incident on a hydrogenated silicon site to 0.025, 0.028, 0.038, and 0.052 for substrate temperatures $T_s = 50$, 150, 250, and 350 °C, respectively.

Si_2H_6 sticking coefficient on a hydrogenated silicon surface was reported in the literature to be $\sim 10^{-3}$ (using molecular-beam scattering techniques) at substrate temperatures close to ours.[57,58]

A nitrogen atom incident on a dangling-bond site is expected to have a sticking coefficient of approximately unity.[2] On the other hand, since hydrogen passivates the growing surface, it may be expected that incident nitrogen atom will simply be reflected if it falls on a hydrogen occupied surface site. Therefore, we can approximate the s_c of an incident nitrogen atom to be $1-\Theta$,[49,59,60] where Θ is hydrogen coverage. H bulk concentration was almost constant with thickness (see Table I for H bulk concentration obtained from NRA measurements). So, setting Θ approximately equal to hydrogen concentration, we estimate the nitrogen sticking coefficients to be 0.72, 0.73, 0.77, and 0.82 at substrates temperatures 50, 150, 250, and 350 °C, respectively.

Similarly, if SiH_3 or Si_2H_6 molecule is incident on a nitrogen site, we may use the same approximation that we used to determine s_c of nitrogen. Therefore, the sticking coefficients of SiH_3 and Si_2H_6 incident on a nitrogen site, which may or may not have a hydrogen atom, are expected to be 0.72, 0.73, 0.77, and 0.82 at substrates temperatures 50, 150, 250, and 350 °C, respectively.

D. Surface diffusion

At substrate temperatures below 400 °C, the surface is terminated by hydrogen atoms. SiH_3 adsorbs onto this surface and can diffuses over it, before being incorporated into the film.[3,51,54,56,61]

Okada and Matsumura measured the diffusion length of the deposition species on a Si surface, from the film thickness measurements on a mask structure, at T_s of 300 °C during a silicon nitride growth to be $\sim$40 μm. They also observed that the surface diffusion has an activation-type dependence on the substrate temperature with the activation energy of $\sim$0.1 eV.[62] Surface diffusion may also be activated by the ion bombardment (10–100 V) from the plasma.[19,55,63–66]

Therefore, surface diffusion will be one of the mechanisms that should be included in our growth model.

E. Desorption

Desorption, by either thermal means or ion bombardments, is a possible mechanism in our experiment.[47]

Infrared absorption (IR) measurements showed that SiN_xH_y films by PECVD from the SiH_4-, N_2-, and He-gas mixtures do not contain NH or NH_2 groups.[31,67] On the other hand, a weak SiH group has been observed in these films. Therefore, desorption of NH_3 is not expected to occur during our experiment.

Recombination of SH group and its successive desorption from the surface is quite possible. It has been suggested by some authors that SiH_3 may recombine with another SiH_3 to be desorbed as Si_2H_6.[44,50,53,59] It has also been suggested that SiH_3 radical may combine with a hydrogen atom from a terminated site, and releases a silane molecule into the gas phase, which creates a dangling bond on the surface.[56,68] Buss and co-workers suggested that an adsorbed Si_2H_6 molecule may decompose and desorbs as SiH_4 and H_2.[57]

From the Fourier transform infrared spectroscopy (FTIR) measurements, thermal desorption of H below 400 °C is not believed to occur, but the hydrogen or hydrogen containing molecules within the bulk of the film may diffuse to the surface to be recombined as H_2 or SiH_4, and then desorb.[43,54,69–71]

Therefore, desorption is also expected to have an activation-type dependence on the substrate temperature. Lucovsky *et al.* reported that desorption from PECVD a-Si:H surfaces increases as the substrate temperature is increased.[46]

F. Film composition, structure, and deposition rate

The resulting film is hydrogenated silicon nitride (SiN_xH_y). H bonding shifts from Si to N as the N/Si ratio increases. H is attached to the dangling bonds in the network.[28] Hydrogen concentration obtained from NRA in PECVD nitride films deposited from SiH_4-N_2 has been shown to decrease with increasing substrate temperature (150–380 °C),[72] IR measurements suggest that in a typical silane discharge, H is incorporated into the film mostly by SiH_n species.[38] This is consistent with the observation that hydrogen content in the nitride films from N_2-SiH_4 process is much lower than that of NH_3-SiH_4 process.[37] Since SiH_3 is the dominant specie in our deposition, its sticking coefficient and desorption rate of Si-H molecules at various temperatures should be the relevant parameters that determine the hydrogen concentration of our films. The lower H con-

centration and Si/N ratios at higher substrate temperatures (see Table I) are believed to be due to the enhanced desorption of Si-H molecules.

Higher growth temperature results in an increase in the rate of diffusion of reactive species to the substrate, probably resulting in more dense films and hence a decrease in the deposition rate with increasing temperature.[43,73] Enhanced desorption at higher temperatures may also be the reason of lower deposition rates in our films as the substrate temperature is increased.

G. Analytical model

Obviously, the system is quite complex and no analytical model reported in the literature can be used directly to describe the results. Here we shall attempt to describe the plasma growth process by extending the reemission model developed by Drotar and co-workers.[17–19] The model assumes a two-dimensional surface described by a height function $h(\mathbf{r},t)$. Overhangs are not allowed. The ratio of the mean free path of the incoming particles to the characteristic length of the surface features is assumed to be large (Knudsen number$\gg 1$), which was the case in our experiments. Hence, collisions between particles within the surface features are neglected. It is also assumed that the surface evolves slowly compared to the redistribution of flux due to the surface features (e.g., within the time it typically takes for a reemitted particle to go from one point on the surface to another, the surface does not change much). The probability of an incoming particle sticking to the surface is s_0 ($0\leqslant s_0 \leqslant 1$), where s_0 is called the zeroth-order sticking coefficient. Incoming particles are called zeroth-order particles, while an nth-order particle that has been reemitted is called an $(n+1)$th-order particle. The probability of an nth-order particle sticking is s_n ($0\leqslant s_n \leqslant 1$), and if the particle does not stick (this has a probability $1-s_n$), then it will be reemitted (in other words, the flux is redistributed). The overall flux of nth-order particles at the in-plane position $\mathbf{r}$ at time t is denoted by $F_n(\mathbf{r},t)$. A detailed description of the characteristics of F_n and the concept of the reemission mode is given in Ref. 17. The growth model for a single type of material film has the form

$$\frac{\partial h}{\tau t}=\nu\nabla^2 h-\kappa\nabla^4 h+\sqrt{1+(\boldsymbol{\nabla}h)^2}[s_0F_0(\mathbf{r},t)+s_1F_1(\mathbf{r},t)+\cdots]+\eta, \tag{1}$$

where the first, second, and last terms are the condensation/evaporation, surface diffusion, and noise terms, respectively. The first term will play the role of desorption in our growth model. The inherent noise in the growth process satisfies

$$\langle \eta(\mathbf{r},t)\rangle=0, \text{ and} \tag{2}$$

$$\langle \eta(\mathbf{r},t)\,\eta(\mathbf{r}',t')\rangle=2A\,\delta(\mathbf{r}-\mathbf{r}')\,\delta(t-t'), \tag{3}$$

where A is proportional to the root-mean square value of the noise term. The factor $\sqrt{1+(\boldsymbol{\nabla}h)^2}$ in Eq. (1) implies that the growth takes place normal to the surface. The main difficulty lies in finding each F_n. An analytical form of F_n has been proposed that takes into account reemission modes and shadowing effects.[17,18]

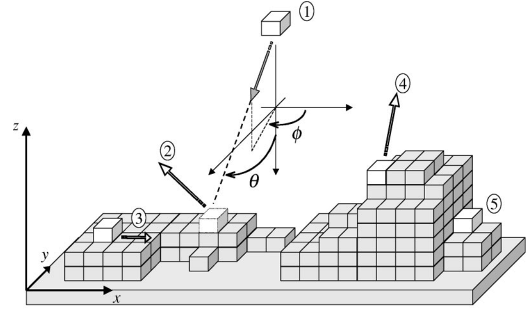

FIG. 6. Some basic processes in the Monte Carlo simulation: (a) A particle of type k, which has an emission probability P_k, is sent towards a surface with angles θ and ϕ. This particle sticks to the surface with probability s_{0k}. (b) If the particle does not stick, then it is reemitted. If it finds another surface feature on its way it may stick there with probability s_{1k}. The reemission process goes on like this for higher-order particles, too. (c) An adatom can diffuse on the surface. (d) A surface atom can desorb. (e) Some surface points are shadowed from the incident and reemission fluxes of particles due to the nearby higher surface features.

For a growth including various types of particles one can extend Eq. (1) to give

$$\frac{\partial h}{\partial t}=G_1+G_2+G_3+\cdots+\eta, \tag{4}$$

where

$$G_k=\nu_k\nabla^2 h-\kappa_k\nabla^4 h+\sqrt{1+(\nabla h)^2}[s_{0k}F_{0i}(\mathbf{r},t)+s_{1k}(\mathbf{r},t)+\cdots] \tag{5}$$

for the k specie during growth. Another complication arises from the fact that each ν_k, κ_k or s_{nk} of type k specie may depend on what site that the specie k is in contact with.

H. Monte Carlo simulation

Numerical computation times of Eq. (4) are quite long for a reasonable scaling to take place. Instead, we used Monte Carlo method to simulate the growth corresponding to the mechanism given by Eq. (4). A summary of basic growth processes is sketched in Fig. 6. Briefly, the simulation proceeds according to a simple set of rules. A single particle of type k with an emission probability P_k and with a position described by x, y, and z is introduced. In this work we will include only three types of species with $k=1,2,3$ corresponding to SiH_3, Si_2H_6 and N, respectively. Although each of these species has a different molecular size, for simplicity we will represent them with particles all having the unit size 1. Since, our model is not an atomic-size-scale model, this approximation should not affect the analysis in our length scales of interest. The position of the particle k is assigned to be random (uniformly distributed) variables x and y, while z is set to the maximum height of the surface, plus 1. The direction of the particle follows the distribution

$dP(\theta,\phi)/d\Omega=\cos\theta/\pi$, where ϕ is the angle of the projection of the particle's trajectory in the xy plane, θ is the angle between the particle's trajectory and the negative z axis, and $d\Omega$ is equal to $d(\cos\theta)d\phi$. This type of flux distribution can represent a typical flux of (PE) CVD process.[74] We used a square lattice surface model that is much faster than off-lattice models and can equivalently simulate amorphous structures.[21,22] The particle moves in a straight line until it hits the surface then it is either deposited ($h\rightarrow h+1$) with probability s_{nk} or is reemitted according to the thermal reemission mode. The particle then travels in a straight line until it hits the surface again or heads away from the surface (in other words, z equals the maximum of the surface plus one). The nth-order sticking coefficient of particle k depends on what surface site it heads on. The particle is allowed to continue bouncing off the surface until it is deposited on the surface or heads away from the surface.

Once the particle k is deposited, a prescribed number of surface atoms, being set to D/F, are randomly picked to become candidates for diffusion. Here, D denotes the number of surface atoms that are available to diffuse within the unit time interval, in which F atoms are deposited to the surface. Therefore, at a time step of a deposited single particle ($F=1$), the surface can, at most, have D/F diffusing atoms. In this way, the ratio of diffusion to deposition strength is adjusted (see the discussion given on p. 176 of Ref. 21). The diffusing surface atom can jump to a nearby site with a probability proportional to $\exp[-(E_D+nnE_N)/k_BT_s]$. Here E_D is the activation energy for diffusion, E_N is the bonding energy with a nearest neighbor, and nn is the number of nearest neighbors. k_B stands for the Boltzmann constant. The particle goes on jumping until it finds an island of atoms, a kink site, a valley, or any lattice point, where (E_D+nnE_N) becomes large and the diffusion probability becomes small. The diffusing particle is prohibited from making a single jump up to a site where the height change is more than one lattice atom. But it can diffuse all the way down to surface valleys at any time (i.e., we should have $\Delta h\leqslant 1$).

After D/F atoms have been checked for diffusion, now we come to the desorption step. Similar to the diffusion mechanism, $\mathcal{D}_{\mathrm{Des}}/F$ number of atoms are given a chance to desorb from the surface. The desorption probability is also proportional to $\exp[-(E_{\mathrm{Des}}+nnE_N)/k_BT_s]$, but this time E_{Des} is the activation energy for desorption.

Finally, after the desorption step is done, another particle is allowed to fall on the surface and the whole process is repeated again.

All the s_{nk} of particle type k (SiH_3, Si_2H_6, and N) for $n\geqslant 0$ will be set to the given sticking coefficients in Sec. III C above. All these three types of particles can diffuse on the surface with $E_D=0.05$ eV. On the other hand, due to the reasoning discussed in Sec. III E, only the surface atoms of type $k=1$ and 2 (corresponding SiH_3 and Si_2H_6, respectively) are allowed to desorb with $E_{\mathrm{Des}}=0.05$ eV. Therefore, at higher temperatures, where the desorption of these particles increase, we should expect to get lower Si/N ratios.

We first need the emission probabilities P_k, which is a measure of relative fluxes of each particle type k from plasma to the surface. At low temperatures, almost none of the chosen surface atoms can neither diffuse nor desorb. Therefore, P_k becomes the free simulation parameter to control the relative ratios of deposited particle types. Setting $T_s=50\,^{\circ}$C, we obtained P_k as $P_1=0.60$ (SiH_3), $P_2=0.10$ (Si_2H_6), and $P_3=0.30$ (N), which gave a Si/N ratio $\sim$1.227 consistent with the experimental results. Since our flow rates are high enough, the plasma chemistry are not expected to change at elevated substrate temperatures. Therefore, the relative flux ratios of depositing species are believed to stay constant as the substrate temperature is raised. This allows us to use the same P_k in our simulations at higher substrate temperatures.

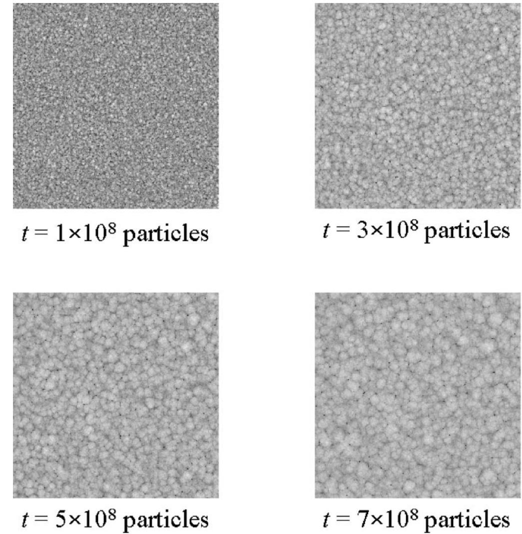

FIG. 7. Four simulated surfaces obtained at $T_s=250\,^{\circ}$C. The surface features become bigger with the increasing simulation time.

After we found the emission probabilities, substrate temperature becomes the critical simulation parameter, just as the case in our experiments. We performed our simulations at substrate temperatures $T_s=50$, 150, 250, and 350 °C. As the temperature is raised more surface atoms become available for diffusion and desorption. We set $D/F=10$ and $\mathcal{D}_{\mathrm{Des}}/F=5$ at all temperatures, which gives Si/N ratios consistent with the ones obtained from experiments. It can be seen from Table I that, as the temperature is raised, the enhanced desorption of Si-type particles lowers the Si/N ratio in simulated films.

Figure 7 shows four simulated surface images obtained at $T_s=250\,^{\circ}$C. We see that these images are quite similar to our AFM images shown in Fig. 2.

Height-height correlation function evolution obtained from the morphologies at various deposition times and temperatures are plotted in Figs. 8(a)–8(d).

The interface width obtained from different substrate temperatures after long simulation times are shown in Fig. 9. As can be seen from Fig. 9, the log-log plot of interface width has a linear part between arrows, from this intermediate times we extract β. Figure 9 also shows that at longer times after the linear part the interface width reaches a saturation point after which it starts fluctuating or does not increase anymore. The dynamic exponent $1/z$ values are obtained

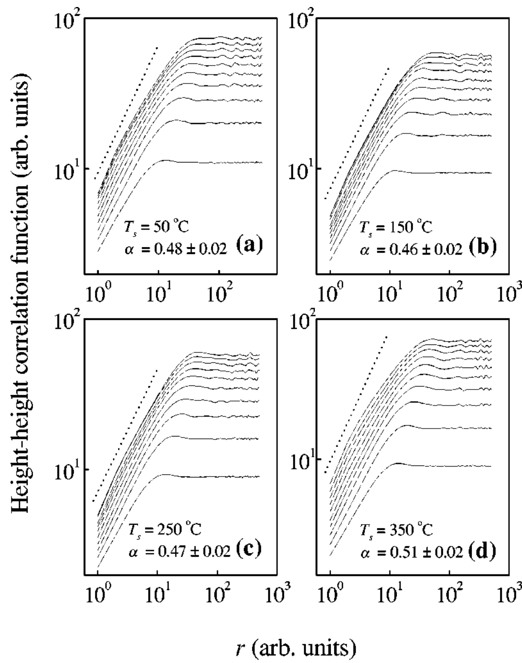

FIG. 8. Simulated equal-time height-height correlation function $H(r,t)$ as a function of the distance r is plotted in log-log scale for $T_s = 50$, 150, 250, and 350 °C in (a), (b), (c), and (d), respectively.

from the log-log plot of ξ versus simulation time t (intermediate times) as shown in Fig. 10.

IV. DISCUSSIONS

Table I summarizes the roughness parameters and Si/N ratios obtained from the simulated surfaces. We see from Table I that the β values obtained from both experiments and simulations agree well. The β values at different substrate temperatures did not change significantly and $\sim$0.40 for both experiments and simulations. At higher temperatures one may expect to get smaller β values due to the smoothening effects of diffusion and desorption. On the other hand, in our case, enhanced desorption of Si-H type of particles reduces the hydrogen coverage, increases the sticking coefficients,

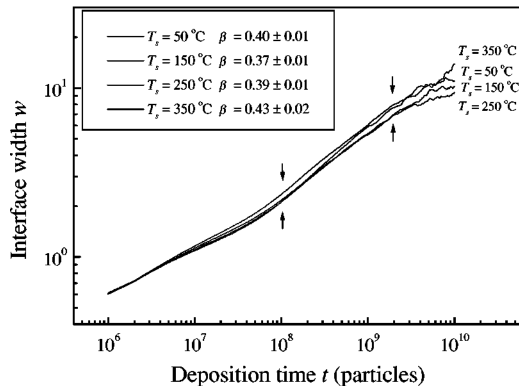

FIG. 9. The interface width w versus growth time t is plotted in log-log scale for various deposition temperatures. β is extracted from the linear part of the plots approximately indicated by arrows after which w reaches the saturation level.

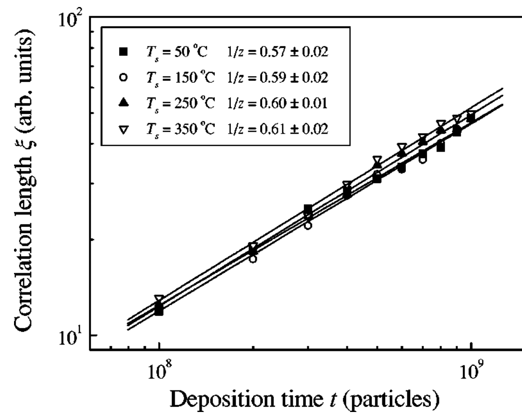

FIG. 10. The lateral correlation length ξ versus growth time t is plotted in log-log scale for various deposition temperatures. The best linear fit gives the dynamic exponent $1/z$.

and therefore incorporates a roughening effect due to the reduced reemission of particles [for the limiting case at which sticking coefficients approach to 1, one gets $\beta \rightarrow 1$ (Refs. 17–19)]. We believe that these two competing mechanisms, a smoothening effect and a roughening effect, result in similar β values even at higher temperatures. Figure 11 briefly summarizes the proposed surface roughening mechanism.

The idea of enhanced desorption and diffusion at elevated temperatures is consistent with the observed inverse substrate temperature dependence of the growth rate in our experiments. Also, the lower values of Si/N ratio at higher substrate temperatures from the simulations agree well with the ones obtained from the experiments. Therefore, the enhanced desorption of Si-H type of particles at higher temperatures may explain the lower growth rates, and lower Si/N and hydrogen concentration values at higher substrate temperatures.

The roughness exponent α and dynamic exponent $1/z$ from the experiments and simulations also did not change sharply with the substrate temperature. $\alpha \sim 0.77$ and ~ 0.48 from experiments and simulations, respectively. The experimental α is higher than that predicted from simulations. However, the true α value after the corrections due to the finite tip effect is expected to be lower than the experimental α. Aue and De Hosson,[24] showed that the surface fractal

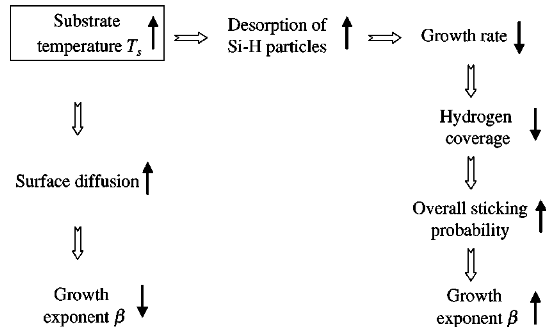

FIG. 11. Possible surface roughening mechanism as the substrate temperature increases. Two pathways that lead to either lowering or raising the growth exponent β.

dimension determined using a scanning probe technique will always lead to an underestimate of the actual scaling dimension or overestimate of the actual roughness exponent, due to the convolution of tip and surface (fractal dimension d_f for a $1+1$ interface is related to α by $d_f = 2-\alpha$). The analysis of Aue and De Hosson included tips with different shapes and aspect ratios. Their analysis for a tip similar to what we used suggests that the true α ranges from 0.6–0.7 for a measured value of 0.77 ± 0.03. $1/z$ from the experiments $\sim$0.28 is lower than $\sim$0.59 obtained from the simulations. If we use the corrected α value, the scaling relation $z=\alpha/\beta$ still does not seem to be able to describe our experimentally observed exponents, suggesting a nonstationary growth mechanism.[23]

V. CONCLUSIONS

In conclusion, the dynamic growth front roughening of amorphous silicon nitride films prepared by a PECVD system using a $SiH_4/N_2/He$ gas mixture was presented. The morphology of the films at different deposition times and substrate temperatures was measured using AFM. A scaling hypothesis has been used to describe the measured exponents $\alpha\sim0.77$, $\beta\sim0.40$, and $1/z\sim0.28$, which did not change significantly with the substrate temperature. None of the well known growth models describes the scaling exponents we obtained.

We used an extended reemission model having a nonlocal nature to describe our results. The model includes the reemission of particles, surface diffusion, desorption, and uncorrelated noise effects. For faster computation times, we used Monte Carlo code to simulate the growth process. We estimated that the dominant depositing species in our experiments were SiH_3, Si_2H_6, and N. Each specie had its own substrate-temperature-dependent sticking coefficients. Simulations with a cosine distribution type of incident flux, surface diffusion, and desorption, in which only Si-H type of particle are allowed to desorb, gave $\alpha\sim0.48$, $\beta\sim0.40$, and $1/z\sim0.59$. The growth exponent β agrees very well with the experimental result. The higher and the lower values of the experimentally obtained α and $1/z$, respectively, compared with that of simulations can be partially attributed to the AFM tip artifact. If the tip effect is considered, the α value is estimated to be $\sim$0.65, closer to the simulated value. Even after this enhancement, simulated α and $1/z$ values are not close enough to the experimental results. This suggests that the simulation work still needs to be improved. Especially, there is a need for more accurate experimental sticking coefficients to be used in the simulations.

In spite of the complicated nature of plasma deposition, our model is shown to reasonably describe the experimental results.

ACKNOWLEDGMENTS

We thank A. Kumar and A. N. U. Roy for performing RBS and NRA measurements. This work was supported in part by NSF. T. Karabacak was supported by the Harry E. Meiners Program.

*Electronic mail: karabt@rpi.edu

[1] D. L. Smith, A. S. Alimonda, C.-C. Chen, S. E. Ready, and B. Wacker, J. Electrochem. Soc. **137**, 614 (1990).

[2] D. L. Smith, A. S. Alimonda, and F. J. von Preissig, J. Vac. Sci. Technol. B **8**, 551 (1990).

[3] J. N. Chiang and D. W. Hess, J. Electrochem. Soc. **137**, 2222 (1989).

[4] S. Meikle and Y. Hatanaka, Appl. Phys. Lett. **57**, 762 (1990).

[5] F. H. P. M. Habraken and A. E. T. Kuiper, Mater. Sci. Eng., R. **12**, 123 (1994).

[6] D. R. Cote, S. V. Nguyen, A. K. Stamper, D. S. Armbrust, D. Tobben, R. A. Conti, and G. Y. Lee, IBM J. Res. Dev. **43**, 5 (1999).

[7] H. Meiling, E. Ten Grotenhuis, W. F. Van Der Weg, J. J. Hautala, and J. F. M. Westendorp, in Amorphous Silicon Technology-1996, edited by M. Hack *et al.*, Mater. Res. Soc. Symp. Proc. No. 420 (Material Research Society, Pittsburgh, 1996), p. 99.

[8] G. Turban, Pure Appl. Chem. **56**, 215 (1984).

[9] H. F. Winter, *Topics in Current Chemistry: Plasma Chemistry III*, edited by S. Verpek and M. Venugopulan (Springer-Verlag, Berlin, 1980), pp. 65–112.

[10] G. Carter and G. S. Calligan, *Ion Bombardment of Solids* (American Elsevier, New York, 1969).

[11] J. R. Hollahan and A. T. Bell, *Techniques and Applications of Plasma Chemistry* (Wiley, New York, 1974).

[12] H. Dun, P. Pan, F. R. White, and R. W. Douse, J. Electrochem. Soc. **128**, 1555 (1981).

[13] W. A. P. Claassen, Plasma Chem. Plasma Process. **7**, 109 (1987).

[14] A. Yuuki, Y. Matsui, and K. Tachibani, Jpn. J. Appl. Phys., Part 1 **28**, 212 (1989).

[15] S. Miyazaki, Y. Kiriki, Y. Inoue, and M. Hirose, Jpn. J. Appl. Phys., Part 1 **30**, 1539 (1991).

[16] C.-P. Chang, C. S. Pai, and J. J. Hsieh, J. Appl. Phys. **67**, 2119 (1990).

[17] J. T. Drotar, Y.-P. Zhao, T.-M. Lu, and G.-C. Wang, Phys. Rev. B **61**, 3012 (2000).

[18] J. T. Drotar, Y.-P. Zhao, T.-M. Lu, and G.-C. Wang, Phys. Rev. B **62**, 2118 (2000).

[19] T. Karabacak, Y.-P. Zhao, G.-C. Wang, and T.-M. Lu, Phys. Rev. B **64**, 085323 (2001).

[20] *Dynamics of Fractal Surfaces*, edited by F. Family and T. Vicsek (World Scientific, Singapore, 1991).

[21] A.-L. Barabási and H. E. Stanley, *Fractal Concepts in Surface Growth* (Cambridge University, Cambridge, 1995).

[22] P. Meakin, *Fractals, Scaling, and Growth Far from Equilibrium* (Cambridge University Press, Cambridge, 1998).

[23] T.-M. Lu, H.-N. Yang, and G.-C. Wang, in *Fractal Aspects of Materials*, edited by F. Family, B. Sapoval, P. Meakin, and R. Wool, Mater. Res. Soc. Symp. Proc. No. 367 (Material Research Society, Pittsburgh, 1995), p. 283.

[24] J. Aue and J. Th. M. De Hosson, Appl. Phys. Lett. **71**, 1347 (1997).

[25] G. S. Bales, A. C. Redfield, and A. Zangwill, Phys. Rev. Lett. **62**, 776 (1989).

[26] K. Wasa and S. Hayakawa, *Handbook of Sputter Deposition Technology* (Noyes, New Jersey, 1992).

[27] A. Grill, *Cold Plasma in Materials Fabrication* (IEEE, New York, 1994), Chap. 3.
[28] D. L. Smith, J. Vac. Sci. Technol. A **11**, 1843 (1993).
[29] B. Chapman, *Glow Discharge Processes* (Wiley, New York, 1980), Chap. 2.
[30] T. Fuyuki, IEICE Trans. Electron. **E75-C**, 1013 (1992).
[31] D. V. Tsu, G. Lucovsky, and M. J. Mantini, Phys. Rev. B **33**, 7069 (1986).
[32] T. M. Klein, T. M. Anderson, A. I. Chowdhury, and G. N. Parsons, J. Vac. Sci. Technol. A **17**, 108 (1999).
[33] J. Campmay, J. L. Andujar, A. Canillas, J. Cifre, and E. Bertran, Sens. Actuators A **37–38**, 333 (1993).
[34] M. J. Loboda and J. A. Seifferly, J. Mater. Res. **11**, 391 (1996).
[35] P. Roca i Cabarrocas, in Amorphous Silicon Technology-1989, edited by A. Madan *et al.*, Mater. Res. Soc. Symp. Proc. No. 149 (Material Research Society, Pittsburgh, 1989), p. 33.
[36] G. N. Parsons, J. H. Souk, and J. Batey, J. Appl. Phys. **70**, 1553 (1991).
[37] J. H. Souk, G. N. Parsons, and J. Batey, in *Amorphous Silicon Technology*-1991, edited by A. Madan *et al.*, Mater. Res. Soc. Symp. Proc. No. 219 (Material Research Society, Pittsburgh, 1991), p. 787.
[38] G. Lucovsky and D. V. Tsu, J. Vac. Sci. Technol. A **5**, 2231 (1987).
[39] P. G. Pai, S. S. Chao, Y. Takagi, and G. Lucovsky, J. Vac. Sci. Technol. A **4**, 689 (1986).
[40] A. A. Bright, J. Vac. Sci. Technol. A **9**, 1088 (1991).
[41] J. Batey, E. Tierney, J. Stasiak, and T. N. Nguyen, Appl. Surf. Sci. **39**, 1 (1989).
[42] J. Batey and E. Tierney, J. Appl. Phys. **60**, 3136 (1986).
[43] M. Gupta, V. K. Rathi, R. Thangaraj, and O. P. Agnihotri, Thin Solid Films **204**, 77 (1991).
[44] A. Gallagher, in *Plasma Synthesis and Etching of Electronic Materials*, edited by R. P. H. Chang and B. Abeles, Mater. Res. Soc. Symp. Proc. No. 39 (Material Research Society, Pittsburgh, 1985), p. 99.
[45] A. Gallagher, Phys. Rev. E **62**, 2690 (2000).
[46] G. Lucovsky, D. V. Tsu, and G. N. Parsons, in *Deposition and Growth: Limits for Microelectronics*, edited by G. W. Rubloff, AIP Conf. Proc. No. 167 (AIP, New York, 1988), p. 156.
[47] D. L. Smith, *Thin-Film Deposition: Principles and Practice* (McGraw-Hill, New York, 1995).
[48] Z. M. Qian, H. Michiel, A. Van Ammel, J. Nijs, and R. Mertens, J. Electrochem. Soc. **135**, 2378 (1988).
[49] J. Perrin and T. Broekhutzen, in *Photon, Beam, and Plasma Stimulated Chemical Processing at Surfaces*, edited by Vincent M. Donnelly *et al.*, Mater. Res. Soc. Symp. Proc. No. 75 (Material Research Society, Pittsburgh, 1987), p. 201.
[50] J. Perrin and T. Broekhuizen, Appl. Phys. Lett. **50**, 433 (1987).
[51] J. Perrin, Y. Takeda, N. Hitano, Y. Takeuchi, and A. Matsuda, Surf. Sci. **210**, 114 (1989).
[52] A. Gallagher, J. Appl. Phys. **63**, 2406 (1988).
[53] R. Robertson and A. Gallagher, J. Appl. Phys. **59**, 3402 (1986).
[54] J. Robertson, J. Non-Cryst. Solids **266–269**, 79 (2000).
[55] P. Roca i Cabarrocas, in *Amorphous Silicon and its Alloys*, edited by T. Searle (Inspec, England, 1998), Chap. 1.
[56] A. J. Flewitt, J. Robertson, and W. I. Milne, J. Non-Cryst. Solids **266–269**, 74 (2000).
[57] R. J. Buss, P. Ho, W. G. Breiland, and M. E. Coltrin, in *Deposition and Growth: Limits for Microelectronics* (Ref. 46), p. 34.
[58] R. J. Buss, P. Ho, W. G. Breiland, and M. E. Coltrin, J. Appl. Phys. **63**, 2808 (1988).
[59] M. J. McCaughey and M. J. Kushner, Appl. Phys. Lett. **54**, 1642 (1989).
[60] C. C. Tsai, J. G. Shaw, B. Wacker, and J. C. Knights, in *Amorphous Silicon Semiconductors—Pure and Hydrogenated*, edited by A. Madan *et al.*, Mater. Res. Soc. Symp. Proc. No. 95 (Material Research Society, Pittsburgh, 1987), p. 219.
[61] D. M. Tanenbaum, A. L. Laracuente, and A. Gallagher, Phys. Rev. B **56**, 4243 (1997).
[62] S. Okada and H. Matsumura, in *Amorphous and Crystalline Insulating Thin Films*-1996, edited by W. L. Warren *et al.*, Mater. Res. Soc. Symp. Proc. No. 446 (Material Research Society, Pittsburgh, 1987), p. 109.
[63] C.-P. Chang, D. L. Flamm, D. E. Ibbotson, and J. A. Mucha, J. Vac. Sci. Technol. B **6**, 524 (1988).
[64] D. L. Flamm, J. Vac. Sci. Technol. A **4**, 729 (1986).
[65] R. F. Bunshah and R. S. Juntz, J. Vac. Sci. Technol. **9**, 1404 (1972).
[66] B. Drevillon and M. Toulemonde, J. Appl. Phys. **58**, 535 (1985).
[67] D. V. Tsu and G. Lucovsky, J. Vac. Sci. Technol. A **4**, 480 (1986).
[68] E. R. Austin and F. W. Lampe, J. Phys. Chem. **80**, 2811 (1976).
[69] W. Beyer, J. Non-Cryst. Solids **198**, 40 (1996).
[70] P. Gupta, V. L. Colvin, J. L. Brand, and S. M. George, in *Deposition and Growth: Limits for Microelectronics* (Ref. 46), p. 50.
[71] C. Boehme and G. Lucovsky, J. Appl. Phys. **88**, 6055 (2000).
[72] R. Chow, W. A. Lanford, W. Ke-Ming, and R. S. Rosler, J. Appl. Phys. **53**, 5630 (1982).
[73] A. K. Sinha, H. J. Levistein, T. E. Smith, G. Quintana, and S. E. Haszko, J. Electrochem. Soc. **125**, 601 (1978).
[74] T. S. Cale and V. Mahadev, in *Modeling of Film Deposition for Microelectronic Applications*, edited by S. Rossnagel and A. Ulman, Thin Films Vol. 22 (Academic, San Diego, 1996), p. 175.